Integrating induced seismicity with rock mechanics: a conceptual model for the 2011 Preese Hall fracture development and induced seismicity

Rob Westaway
School of Engineering, University of Glasgow,
James Watt (South) Building, Glasgow G12 8QQ, U.K.

e-mail: robert.westaway@glasgow.ac.uk

Supplementary material

Contents:

1. Stratigraphy, structural geology, and rock-mechanical properties

Northern England is formed from a mosaic of Carboniferous sedimentary basins inset into metasedimentary 'basement', which was metamorphosed during the Lower Palaeozoic Caledonian Orogeny (e.g., Fraser et al., 1990; Kirby et al., 2000; Andrews, 2013). These basins underwent extension as a result of Dinantian (Early Carboniferous) tectonics (e.g., Fraser and Gawthorpe, 2003; Waters and Davies, 2006), followed by continued sedimentation during the subsequent 'thermal subsidence' phase of basin development in the Silesian (Late Carboniferous). The region depicted in Fig. 2 thus includes, amongst others, the Bowland, Cheshire, Cleveland, and Gainsborough Basins, all recognized as potential shale gas plays (e.g., Andrews, 2013). This resource is in hemipelagic shale that the British Geological Survey (BGS) has informally named the 'Bowland-Hodder Unit' (Fig. 2). In the Bowland Basin these rocks fall within the established Craven Group (Waters et al., 2011; Andrews, 2013); at Preese Hall the 'Upper Bowland-Hodder Unit' is equivalent to the established Bowland Shale Formation, the 'Lower Bowland-Hodder Unit' corresponding to the established Hodder Mudstone Formation (cf. Fig. 5(a)). Deposited primarily during the Visean stage (but locally also encompassing the late Tournaisian and/or early Namurian) of the Dinantian in relatively deep-water environments in normal-fault hanging-walls, these rocks pass laterally in footwall settings into the more familiar shallow-water carbonate facies that forms much of the outcrop in upland parts of northern England, such as the Yorkshire Dales and the White Peak uplands of Derbyshire (Fig. S1.1).

Thus, in the region covered by Fig. S1.1, the Bowland Basin is bounded to the NE by the South Craven Fault and subparallel North Craven Fault, which separate it from the up-faulted Askrigg Block, and to the southeast by the Pendle Fault, which also delineates the Central Lancashire High in its footwall. The South Craven Fault continues SE as the Morley-Campsall Fault (or Aire Valley Fault), which separates the Gainsborough Basin to the southwest from the Askern-Spitall High to the northeast. The aforementioned Askrigg Block is bounded to the WNW by the Dent Fault and to the NNE by the Stockdale Fault, the hanging-wall of which contains the Stainmore Basin. The latter continues eastward into the Cleveland Basin, bounded to the south by the Flamborough Head - Vale of Pickering Fault Zone with the Market Weighton High in its footwall. The Askrigg Block is underlain by Caledonian granite; this is now thought to date from the Caradocian stage of the Ordovician (e.g., Pharaoh et al., 1997; Millward, 2006), rather than the Devonian age formerly adopted (e.g., Dunham, 1974; Dunham and Wilson, 1985). The Market Weighton High is inferred to also have a granite core from gravity studies (e.g., Bott et al., 1978; Bott, 1988). The relative buoyancy of the granites beneath these

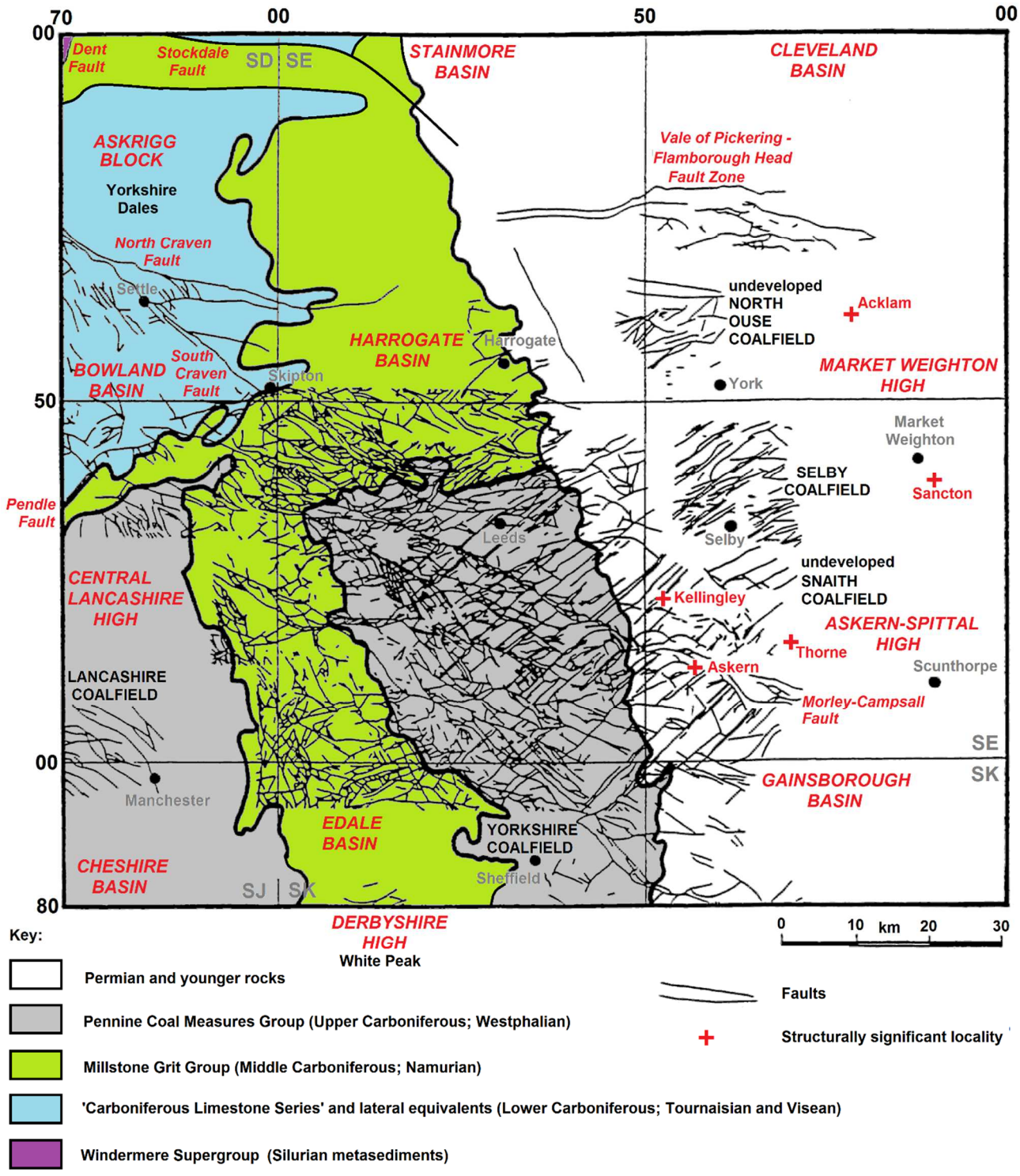

Figure S1.1. *Map of the eastern part of the area in Fig. 2, likewise indexed to the BNG, showing faults and fractures documented primarily as a result of detailed studies related to coal mining. The outcrop boundaries depicted are simplified. The Alston Block is located north of the Stainmore Basin, being bounded to the south by the Butterknowle Fault (e.g., Chadwick et al., 1995; Kimbell et al., 2010). The structural significance of each of the sites marked is explained by British Coal Corporation (1997); for example, Acklam and Sancton mark hinge zones at the northern and southern margins of the Market Weighton High. Kellingley Colliery, one of the sites thus depicted, was also the last deep coal mine in Britain, coal production there having ended in December 2015. Modified from Fig. 2.1(a) of British Coal Corporation (1997).*

and other parts of Britain has long been recognized as a major factor influencing both ancient and active patterns of vertical crustal motion (e.g., Bott, 1988; Waters and Davies, 2006; Westaway, 2017). It is traditional in Britain to associate structural trends with ancient geological events. Thus (e.g., Hills, 1966), a SW-NE orientation is regarded as 'Caledonide' and a NW-SE or 'Charnoid' orientation is associated with the concealed Caledonides beneath eastern England (e.g., Pharaoh et al., 2011). A north-south structural trend is designated as 'Malvernoid' after the Precambrian rocks of the Malvern Hills in west-central England, and a west-east trend as 'Armoricanoid' or Variscan. Although other orientations are also present, the majority of the major structures in Fig. S1.1 strike SW-NE or NW-SE, suggesting that they reflect Carboniferous reactivation of Caledonian-age basement structures (e.g., Waters and Davies, 2006). Any assessment of the conditions that might result in induced seismicity under the present-day stress field (discussed below) must consider this diversity of structural trends, and the associated multiplicity of orientations of potential planes of weakness within the crust.

In addition to these major structures, Figure S1.1 also indicates the density of faults and fractures in this region. Its coverage is uneven, there being much more detail in former coalfields and areas where the coal resource was explored but not exploited. Where no exploration or production of coal has taken place, there is a typical lack of correspondingly detailed investigation. Similar structural detail exists in the former metalliferous mining regions of the Askrigg and Alston Blocks of the central and northern Pennines (e.g., Turner et al., 1995; Fig. S1.1); however, these upthrown Carboniferous footwall blocks are not directly relevant to shale gas prospecting. The case study of the Selby coalfield, developed starting in the 1970s and discussed by British Coal Corporation (1997), is pertinent to demonstrating the influence of structural complexity on resource extraction. Shortly after coal production began in the 1980s, it was realised that this coalfield is pervasively faulted, many faults having throws below resolution limit of 1970s-era seismic reflection surveys. Repeat surveys in the 1990s, with resolution of 2 ms two-way-time or ~3 m of throw, revealed many additional faults (Fig. S1.1); faults with even small throws of this order proved to be severe impediments to the economical operation of coal-cutting machinery. Indeed, this coalfield was shut down completely by 2004 after only 121 million tonnes had been mined from a single seam, the estimated coal reserves being ~400 million tonnes from this seam and ~6000 million tonnes in total.

Despite the main phase of crustal extension in the region having ended circa the end Dinantian, many faults that had been active at this time also offset younger rocks, indicating multiple phases of subsequent minor extension and/or crustal shortening as well as the significant phase of crustal shortening during the Variscan orogeny (e.g., Waters et al., 1994; Kirby et al., 2000; De Paola et al., 2005; Waters and Davies, 2006; Pharaoh et al., 2011). It has long been recognized that coal mine records, such as those summarized in Fig. S1.1, provide much more detail than is available to the petroleum industry from seismic surveys (e.g., British Coal Corporation, 1997); these also provide information regarding the relative chronologies of slip on the different sets of faults in Fig. S1.1. It is thus evident that slip on SW-NE-striking faults was either synchronous with or younger than the youngest slip on the NW-SE-striking Morley-Campsall Fault. Other SW-NE-striking faults are themselves offset by strike-slip displacements on E-W-striking faults, which appear to indicate the most recent phase of slip and indicate a stress field orientation very different from that during the Carboniferous (see below). Similar complexities are evident in parts of northern England to the north of Fig. S1.1; mine records and geophysical surveys indicate that the most recent deformation has involved left-lateral slip on NE-SW-striking faults (e.g., Robson, 1964, 1977; Turner et al., 1995). The disposition of cave levels in the limestone uplands of the Yorkshire Dales (Askrigg Block) and White Peak uplands indicate that, since the start of the Middle Pleistocene, these regions have experienced uplift at ~0.2 mm a^{-1}, faster than in the lowland regions to the east and south (e.g., Westaway, 2009, 2015b, 2017; Bridgland et al., 2014; Westaway et al., 2015). These analyses also indicate correlations between present-day vertical crustal motions and some of the crustal blocks depicted in Fig. S1.1, for example the Cleveland Basin now appears to be uplifting faster than the Market Weighton High farther south. These patterns of progressive vertical crustal motion are also modulated by the transient isostatic effects of multiple cycles of loading and unloading by ice sheets (e.g.,

Bridgland et al., 2010). The abundant evidence now available for widespread active crustal deformation within Britain bears upon how one interprets *in situ* stress data within the crust (see below).

A significant feature of the Preese Hall-1 case study was the deformation to the wellbore noted following the largest of the induced earthquakes (e.g., de Pater and Baisch, 2011). Caliper tool measurements reported by de Pater and Baisch (2011) indicate that this deformation was concentrated between depths (MD) of 8502 and 8626 ft or 2590-2636 m, which correspond to ~2552-2593 m (TVD) (the procedure used in this study for converting between these two measures of depth for this well is explained in the main text); this deformed interval is identified as a white band on the well track in Fig. 4. It occurs within rocks that were thought at the time to be the 'Hodder Mudstone'; this part of the sequence is evidently thinner in the vicinity of the Preese Hall-1 well than elsewhere (Fig. 4), indicating that it has experienced localized deformation. Weak zones sub-parallel to the bedding were indeed recognized in the Preese Hall-1 dataset by de Pater and Baisch (2011) and Harper (2011) and might well have accommodated the observed local thinning by bedding plane slip. Harper (2011) indeed noted that these weak zones make the mechanical properties of this formation anisotropic.

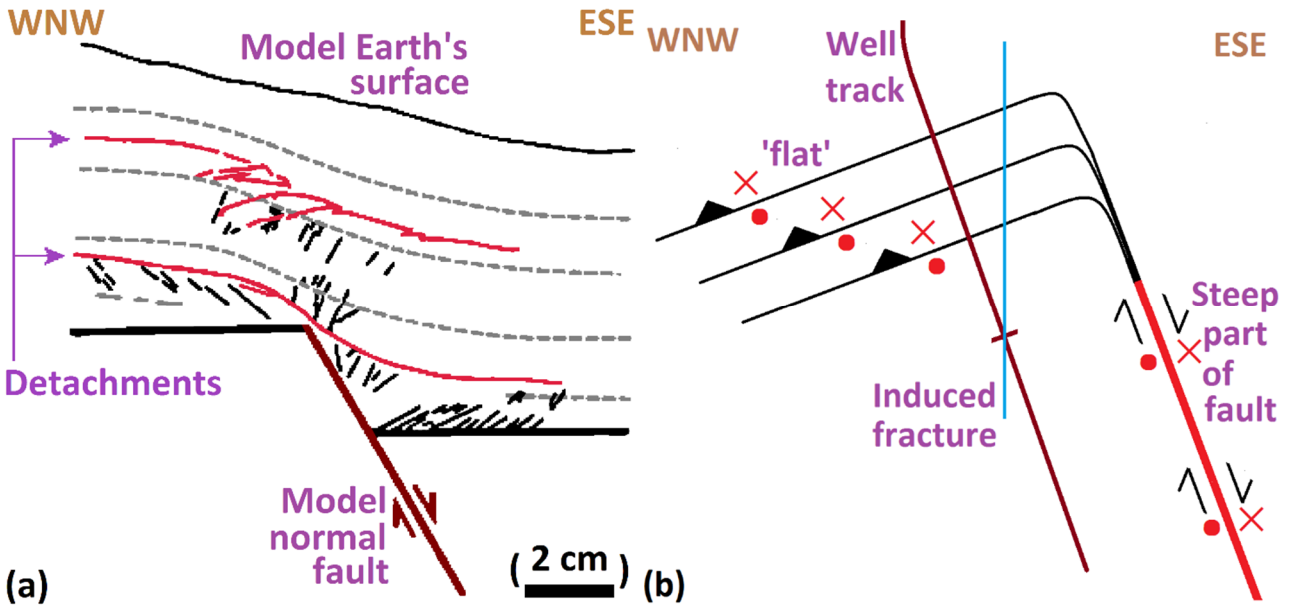

Figure S1.2. *Potential schematic representations, not to scale, but spanning vertical and horizontal distances of up to several hundred metres, of the geometry of faulting associated with the induced seismicity and related wellbore deformation at Preese Hall in 2011.* ***(a)*** *Modified from Fig. 1(b) of Ferrill et al. (2007), based on Fig. 8(f) of Withjack et al. (1990). This diagram, showing development of sub-horizontal 'detachments' with top-to-the-right sense of shear, is based on analogue modelling (at the scale indicated) using a rheologically layered model (with dashed lines denoting 'form lines' within the model, which were horizontal prior to fault slip), in which the detachments were simulated by placing pairs of acetate sheets within the model. Note also the presence in the model of the free surface representing the Earth's surface, which is a requirement for this particular style of deformation to occur.* ***(b)*** *Modified from Fig. 1 of Westaway (2016b); unlike that in (a), this variant does not require an adjacent free surface. The predominant sense of slip on this model fault plane was left-lateral, indicated with dot and cross symbols to denote motions in and out of the section plane, together with a minor component of normal slip, indicated by paired arrows. Curved lines extending from the updip end of the steep part of the fault indicate schematically the 'horsetail splay' or 'contractional imbricate fan' forming the 'flat' at its termination, which is inferred on the basis of the 'bedding plane slip' that caused the deformation to the Preese Hall-1 wellbore. The strike-slip component of motion on the steep part of the fault is thus accommodated by top-to-the-NNE bedding plane slip on this 'flat', again represented by dot and cross symbols, whereas its normal component of slip is accommodated by contraction, perpendicular to the bedding planes, represented by chevron symbols.*

It is shown in the main text that the presence of this subhorizontal zone of disrupted stratigraphy, or zone of weakness, at ~2550-2590 m depth (TVD), is key to understanding why the Preese Hall project 'went wrong'. The calculations indicate that high net pressure of fracking fluid 'opened' this structure, resulting in horizontal migration of fracking fluid. It is thus of interest to consider why this zone is there; this bears, for example, upon the probability of repetition of similar issues during future fracking projects. One possibility, as Harper (2011) has suggested, is that the zone marks a syn-sedimentary submarine landslide, Gawthorpe and Clemmey (1985) having documented such structures elsewhere in the Bowland Shale. However, this would imply that the presence of this zone near a steep normal fault is coincidental, implying that the co-occurrence of coseismic slip and wellbore deformation was, likewise, a coincidence, and thus lacking in wider significance. A second possibility, after Ferrill et al. (2007), is that the zone is a 'detachment', mechanically and geometrically related to slip on the adjacent steep fault, as illustrated in Fig. S1.2(a). However, the Ferrill et al. (2007) scenario requires a free surface (i.e., the Earth's surface) in close proximity, which it is not. Figure S1.2(b) illustrates a variant of this, suggested by Westaway (2016b), in which the subhorizontal 'flat' marks the upward termination of the steep fault in a manner that requires no related deformation at shallower depths and, thus, no adjacent free surface. The inferred geometry resembles a conventional 'horsetail splay' (e.g., Sylvester, 1988) or 'contractional imbricate fan' (e.g., Woodcock and Fischer, 1986) fault termination. From consideration of the magnitude (2.3) and, thus, seismic moment, of the largest Preese Hall induced earthquake, a coseismic displacement of ~10 mm can be estimated (cf. Westaway and Younger, 2014); it is envisaged, in terms of the scheme in Fig. S1.2(b), that beyond the up-dip limit of the steep part of the fault, this shear displacement was partitioned across the various planes of weakness within the 'flat'.

One reason why the possibility that the wellbore deformation was mechanically related to the induced seismicity was not recognized sooner was that the Preese Hall-1 operator (whose views are reflected in the Clarke et al., 2014, paper) located the seismicity well east of the wellbore (Figs 1, 4). This argument was superseded by the realisation of the mistakes in their paper and the resulting adjustment of the position of the seismogenic fault closer to the wellbore, although the patch of it that slipped in the largest induced earthquakes was to the south (Westaway, 2016a; Fig. 1). Another reason was because de Pater and Baisch (2011) were unable to identify a clear conceptual link between the seismogenic fault and the wellbore deformation, notwithstanding the potential links now suggested (Fig. S1.2). Clarke's (2016) comment (cf. Baisch and Vörös, 2011) that 'all of the evidence collected to date supports the observation that the wellbore was within 300 m of a fault but does not intersect it' is therefore debateable, given the clear possibility that the 'flat' in which the wellbore deformation occurred was part of the upward fault termination (Fig. S1.2(b)) or otherwise directly related to this fault (Fig. S1.2(a)). For illustrative purposes within the present work, it will be assumed that this 'flat' is, indeed, the updip termination of the steep fault, in the sense indicated in Fig. S1.2(b). However, from the point of view of the geomechanics, it is immaterial whether it might instead be a 'detachment', related to the fault as in Fig. S1.2(a), or the sole of a submarine palaeo-landslide or a zone of non-cohesive bedding planes that developed for some other reason, coincidentally located near the adjacent fault.

Only limited information is currently available on the mechanical properties of Bowland Shale. Carter and Mills (1974) determined 2-14 GPa for the Young's modulus, 1-8 MPa for the tensile strength S_T and 2-12 MPa for the cohesion S_C, for 24 samples of Middle Carboniferous (Namurian) mudstone from sites in northeast England, which might represent analogues for the Bowland Shale. Harper (2011) summarized results of geomechanical testing of 9 samples of Bowland Shale recovered from the Preese Hall-1 well just below the shallowest perforations for stage 4 of the fracking. These results indicate shear modulus μ 10-20 GPa, bulk modulus 21-52 GPa, and Poisson's ratio ν 0.14-0.30. These elastic moduli are thus rather higher than for Namurian mudstone, suggesting that the latter may not be a good analogue for the Bowland Shale after all (cf. Westaway and Younger, 2014). Harper (2011) also reported the Young's modulus, derived from well logging, for a ~500 m thickness mostly within the Bowland Shale. This varies from ~25-70 GPa, thus broadly consistent with the aforementioned measurements of μ and ν, with a typical value of ~60 GPa; the principal departure from this value, a decrease to ~25-30 GPa, occurs over ~8660-8750 ft (MD) or ~2595-2620 m (TVD)

and coincides with the subhorizontal 'flat' that plays a significant role in the geomechanical model developed in this study. Harper (2011) did not report any measurements of cohesion for 'intact' rock but inferred that pre-existing fractures within the Bowland Shale at Preese Hall are cohesionless (i.e., in the direction parallel to fractures, S_C=0), indicating that this shale (unlike many others) does not ever 'bond back together' once fractured. Most recently, Gao et al. (2015) have reported analyses of what they described as 'typical gas shale rocks in northeastern Ohio'. They did not note, however, whether their samples were of the Carboniferous Marcellus Shale or of older (Lower Palaeozoic) shale. They nonetheless determined a typical density of their samples, whose properties were strongly anisotropic, as 2503 kg m^{-3}. Two groups of samples yielded mean values for tensile strength of 7.4 and 9.1 MPa in the direction perpendicular to the bedding, with bedding-parallel values estimated as 300-360 times smaller (i.e., ~0.02-0.03 MPa). Gao et al. (2015) also measured seismic wave velocities (V_P and V_S) but did not derive elastic properties from these. They determined both V_P and V_S for nine samples, but for three of these the V_P/V_S ratios are so low as to require negative values of ν. Discounting these three data, one obtains V_P/V_S=1.89$\pm$0.79 ($\pm1\sigma$) and ν=0.27$\pm$0.15 ($\pm1\sigma$) for the others, the latter result requiring the standard formula

$$\nu \equiv \frac{(V_P / V_s)^2 - 2}{2(V_P / V_s)^2 - 2}, \qquad \text{(S1.01)}$$

(e.g., equation (A4) of Westaway and Younger, 2014). Although there is much scatter in these data, the results are nonetheless of some value. Of course, to be ideally useful for the present study, measurements such as these should really be made under conditions that simulate the temperature and state of stress at depth and not under ambient conditions in the laboratory. For comparison, using in situ logging, the typical density of the Bowland Shale at Preese Hall was reported as ~2620 kg m^{-3} in Fig. 2 of Baker Hughes (2011).

Currently, relatively little quantitative information is available on the porosity and permeability of Bowland Shale, although many workers have reported the latter parameter as 'low'. As an example, iGas (2014) reported porosity in the range 1.1-2.6% and typical permeability ~0.03 μD (~3×10^{-20} m^2) for Bowland Shale in their Irlam-1 (or Ince Moss; SJ79NW314) well located (at SJ 73615 97552) west of the city of Manchester (Fig. 2). Rutter and Mecklenburgh (2017) report results of more detailed analysis of the shale from this borehole, including porosity 1.9$\pm$0.4% and pressure-dependent permeability. They demonstrate that permeability decreases with effective confining pressure P_e (the difference between confining pressure and pore pressure), being ~0.1 μD for P_e=40 MPa, ~0.04 μD for P_e=60 MPa, and ~0.01 μD for P_e=80 MPa. One might envisage a similar pressure-dependence of permeability of the shale at Preese Hall, but currently there are no published data to substantiate this. Furthermore, given that the Preese Hall site is in deep marine deposits near the axis of an Early Carboniferous depocentre (e.g., Fraser and Gawthorpe, 2003), whereas the Irlam-1 site is in an intra-basinal shallow-marine 'high' (the 'Holme High') where the sediments are generally coarser-grained (iGas, 2014), lower permeability might be anticipated at Preese Hall.

2. Regional state of stress and its implications

Establishing *in situ* stress is key to determining how close to failure any particular fault is. It is well established that, typically in northern England, the maximum principal stress is roughly north-south, with the minimum principal stress roughly east-west and the intermediate principal stress near-vertical (e.g., Evans and Brereton, 1990; Chadwick et al., 1996; Cartwright, 1997; Baptie, 2010; Heidbach et al., 2010), although quite abrupt local variations are nonetheless apparent. The high differential stress $\Delta\sigma$ measured in the Preese Hall-1 well (Fig. 5(b); see also below) is thus no surprise; high $\Delta\sigma$ has long been apparent in Britain, for example from *in situ* stress measurements in coal mines (e.g., Cartwright, 1997; Mark and Gadde, 2008) and at the former Rosemanowes geothermal energy project site in Cornwall (e.g., Pine and Batchelor, 1984; see also below). It has subsequently been realised that the differential stress is sufficient for major faults, causing localized surface deformation, to be active in various parts of Britain (Westaway et al., 2006; Westaway, 2010; Harding et al., 2012); it was already established that the transient stress field during ice unloading at the end of the last ice age caused large earthquakes (e.g., Ringrose, 1989; Stewart et al., 2001). The Kingdon et al. (2016) synthesis of stress field orientations for northern England, based on borehole image

logs, presents results that are similar to previous works, but does not include the underlying raw data and does not address magnitudes of $\Delta\sigma$.

The 1980s Rosemanowes project, which attempted to extract heat using hydraulic fracturing to create paths for water flow through granite, provides a graphic illustration of the need to consider the local stress field before embarking on subsurface engineering works. As Pine and Batchelor (1984) explained, this granite has a set of joints oriented at azimuths ~N20-30°W-~S20-30°E. The existing literature (e.g., Richardson and Solomon, 1979; Froidevaux et al., 1980) reported that in northern France, earthquake focal mechanisms and a few *in situ* stress measurements indicate that the minimum principal stress is roughly subperpendicular to this joint set in Cornwall. However, it was already known that focal mechanisms only provide a rough indication of stress orientation, because the minimum principal stress can lie anywhere within the compressional quadrant (McKenzie, 1969). Nonetheless, it was felt that the design of the Rosemanowes injection and production wells could proceed, without supporting local *in situ* stress measurements, assuming that the injection would open tensile fractures parallel to the existing joint set. It was subsequently found that the induced fractures developed in a different direction, opening via a combination of tensile and shear deformation. Later measurements established that the present-day minimum principal stress is oriented N40°E-S40°W, thus at ~60-70°, rather than 90°, to the joint set; this mismatch, plus the combination of high $\Delta\sigma$ (representative values, at 2 km depth, are maximum, intermediate and minimum principal stresses 71, 52, and 30 MPa, the intermediate principal stress being vertical), was sufficient to make the project to 'go wrong' (Pine and Batchelor, 1984). Despite attempts at redesign, this project was subsequently abandoned, having never produced useable quantities of thermal water (e.g., Richards et al., 1994; Parker, 1999). Development of geothermal energy in the UK was set back for a generation and the perception was thus created, which persists in some quarters (e.g., King et al., 2015), that it is such an inherently 'risky' technology it has no significant potential role in any future renewable energy mix. It is nonetheless evident that the failure of the Rosemanowes project involved narrow margins; had the actual stress field been oriented a little closer to what had been assumed during the project design, it might have worked, and the U.K. might thus now be a leading nation in geothermal energy. The present analysis demonstrates that the Preese Hall project also 'went wrong' only by a narrow margin; this has only become apparent following detailed calculations regarding the state of stress.

Other *in situ* stress data for Britain have been compiled by GFZ (2015) and illustrated on maps many times (e.g., Chadwick et al., 1996; Baptie, 2010). Some sites indicate very high $\Delta\sigma$, an example being the borehole at Morley Quarry near Shepshed, Leicestershire (~52.76°N ~1.30°W; SK 473 183), where, at 1520 m depth, the maximum and minimum principal stresses have been determined (using hydraulic fracturing) as 50.9 and 18.7 MPa (e.g., Chadwick et al., 1996). The high $\Delta\sigma$, 32.2 MPa, at such a shallow depth can be withstood since the rocks are strongly cohesive, being Precambrian quartzite of the Charnwood Forest inlier. Furthermore, the azimuth of the maximum principal stress at this site is reported as N89°W-S89°E (GFZ, 2015), thus subperpendicular to what is typical for Britain (e.g., Baptie, 2010; Heidbach et al., 2010), thereby demonstrating the irregularity of the local stress field (see below). In summary, the high $\Delta\sigma$ measured at Preese Hall (Fig. 5(b)) is precisely what one expects from the regional context.

Musson (2007) claimed that 'there is no continuing active deformation' in Britain and, therefore, no point in attempting to identify individual active faults. This view seems to be based on the notion that the seismicity of Britain is releasing elastic strain energy that had been stored by ancient crustal deformation processes, with no accumulation of elastic strain energy; each earthquake thus de-stresses a patch of fault and so no further events will occur there. This paper post-dates (but does not cite) the Westaway et al. (2006) discovery of the first onshore active fault in Britain, and was therefore immediately obsolete on publication; this fault has evidently slipped many times during the Holocene, let alone during the Pleistocene, not just in the one historical earthquake associated with it. The older literature on the seismicity of Britain indeed documents many earthquakes large enough to have been felt, which occurred in close proximity to fault zones that are known from the geological record, and evidently each involved slip on one of the faults within the respective

zones. Onshore instances relevant to northern England include (with supporting data from http://www.quakes.bgs.ac.uk/historical/query_eq/): the Wensleydale earthquake (M_L 4.4) of 14 January 1933, for which the epicentre (reported by Rowland, 1933; circa SD 903 894) adjoins the Stockdale Fault; the Skipton earthquake (M_L 4.8) of 30 December 1944, for which the epicentre (reported by Versey, 1948, 1949; circa SD 988 404) adjoins the South Craven Fault; and the Kirkby Stephen earthquake (M_L 4.1) of 9 August 1970, for which the epicentre (reported by Browning and Jacob, 1970; circa NY 792 130) adjoins the intersection of the Pennine, Dent and Butterknowle faults. The latter event, which Browning and Jacob (1970) regarded as the largest (their magnitude 4.9) to have occurred onshore in Britain since magnitude determinations began in 1935, was indeed attributed by these authors to slip on the southern part of the Pennine Fault. Furthermore, the North Sea earthquake of 7 June 1931 (M_L 6.1 according to Musson, 2007) occurred ~100 km east of Flamborough Head (circa TB 243 558 according to Versey, 1939), within the offshore continuation of the Vale of Pickering – Flamborough Head Fault Zone. This fault zone has recently gained recognition as playing a significant role in the active crustal deformation of Britain, since it forms the southern boundary of the part of northern England that is experiencing relatively rapid uplift (Bridgland et al., 2014; Westaway et al., 2015; Westaway, 2017). Contrary to Musson's (2007) stated view, crustal deformation is evidently widespread, at laterally varying rates, across Britain and no doubt both responds to and contributes to the observed variability in the sense of stress.

Although *in situ* stress measurements (including the magnitudes and orientations of the principal stresses) were made in the Preese Hall-1 well before fracking began in 2011 (Fig. 5(b)), nothing has been reported to establish that they were used in any assessment of the consequences of the fracking prior to this taking place. However, notwithstanding the report by Baker Hughes (2011) of the maximum principal stress azimuth N7°W-S7°E at Preese Hall from World Stress Map (WSM) data, recent WSM outputs (e.g., Heidbach et al., 2010) in fact report the maximum principal stress oriented circa N35°W-S35°E in northwest England. Furthermore, the raw WSM data (GFZ, 2015) indicate that such outputs are based on interpolation between sparse data of diverse orientations. Thus, for example, at Burton-in-Kendal in SE Cumbria (circa SD 538 785; ~46 km from Preese Hall to ~N21°E), GFZ (2015) notes a measurement of the maximum principal stress azimuth as N13°E-S13°W. Conversely, at Sellafield in west Cumbria circa NY 054 037; ~75 km from Preese Hall to ~N35°W), GFZ (2015) lists nine measurements of the maximum principal stress azimuth from which Westaway (2016a) determined a mean of 156±6° (±2s) or N24±6°W-S24±6°E (±2s). Thus, the maximum principal stress azimuth varies significantly across this region, making it essential to rely on local measurements from the Preese Hall-1 borehole rather than inferences using data from more distant localities. The view has nonetheless been repeatedly stated (e.g., Müller et al., 1992; Heidbach et al., 2010) that, abrupt local variations being absent, the stress field in Britain is determined by boundary conditions resulting from the motions of adjoining plates. On the contrary, the abruptness of the observed local variations in the stress tensor orientation suggests strongly that this argument is wrong, as might well be expected from the recent analyses (e.g., Westaway et al., 2006; Westaway, 2009, 2010, 2015a, 2016a; Harding et al., 2012) which infer that the stress fields in particular localities depend on local conditions, such as the local isostatic balance between sedimentation and erosion. Future assessments to inform shale gas or other developments should therefore not use the argument that the stress field depends only on plate motions but should instead establish it using local evidence.

Regarding the stress field orientation at Preese Hall, in addition to the aforementioned Baker Hughes (2011) dataset, previous analyses of local measurements have given the maximum principal stress azimuth as ~187 or 188° from drilling-induced tensile fractures (Harper, 2011), with a combined dataset of borehole breakouts and drilling-induced tensile fractures giving 188±16° (Harper, 2011). Westaway (2016a) determined mean values of 176±5° (±2s) or N4±5°W-S4±5°E (±2s) for the Baker Hughes (2011) dataset and of 187±3° (±2s) or N7±3°E-S7±3°W (±2s) for the Harper (2011) dataset. These two estimates therefore differ significantly (at a 95% confidence level). Others (e.g., Roche et al., 2015) have noted that the state of stress elsewhere shows significant vertical variations within stratigraphic sequences in which one formation undergoes fracking. It is thus preferable to adopt, for the purpose of geomechanical analyses of the Preese Hall fracking, the result

based on the Harper (2011) dataset, since these data originated from the depth range where the fracking was undertaken, whereas the Baker Hughes (2011) dataset was from shallower depths (Fig. 5(b)). Since hydraulic fractures develop in any isotropic rock in the plane perpendicular to the minimum principal stress, it is expected that these propagated away from the Preese Hall-1 well in the vertical plane oriented N7±3°E-S7±3°W (±2s) (Fig. 1).

The present analysis also requires magnitudes of the principal stresses at Preese Hall. Cuadrilla (2014, p. 49) reported that at 2440 m depth the maximum, intermediate and minimum principal stresses are 73.4 MPa, 62.2 MPa and 43.6 MPa. These values were taken as definitive by Westaway (2015a, 2016a), since an accompanying diagram (Fig. 12 of Cuadrilla, 2014) gave the impression of a concentration of data from this depth and stated that these data came from de Pater and Baisch (2011). It was thus assumed that this Cuadrilla (2014) diagram was obtained by numerically integrating the graphs of stress gradients in Fig. 20 of de Pater and Baisch (2011). However, it is now evident that the stress 'data' reported by Cuadrilla (2014) are in fact a mixture of measurements and predictions. Moreover, no actual data were reported by de Pater and Baisch (2011) from 2440 m or 8005 ft depth. As far as can now be established, the outputs presented by Cuadrilla (2014), which Westaway (2015a, 2016a) treated as 'data', are indeed predictions obtained by numerically integrating the de Pater and Baisch (2011) stress gradient graphs. These data were plotted by Cuadrilla (2014) at depth intervals of 305 m, not because that is where measurements were made, but because that is 1000 ft, the grid interval on the vertical axis of the original de Pater and Baisch (2011) diagram, implying that Cuadrilla (2014) might not have incorporated into their analysis variations in the stress gradients within these intervals. This supposition was checked by numerically integrating these graphs, thus obtaining Fig. 5(b). It is therefore evident (by comparison with Fig. 2(b) of Westaway, 2016a) that the portrayal of these stress data by Cuadrilla (2014) is indeed incorrect, most likely for the reason outlined above. The present analysis gives best estimates of 64.38 MPa, 55.23 MPa and 39.88 MPa for the maximum, intermediate and minimum principal stresses at 2440 m depth (TVD), rather different values from those reported by Cuadrilla (2014); the corresponding values at 2400 m are 63.26 MPa, 54.27 MPa and 39.20 MPa.

3. Theory for fluid injection

The present analysis requires the variations in pressure of the injected fluid at each point of injection. Calculations are necessary here, as these values of bottom hole pressure (BHP) were not measured but have to be calculated from other information, including measurements of well head pressure (WHP). The magnitude of the minimum principal stress, σ_h, at the appropriate depth, from equation (3) can be subtracted from the calculated BHP to determine the net pressure p_o of the injected fluid at its injection point, as a starting point for the calculations relating to hydraulic fracture development (in section 4 of this supplementary material).

From Lyons et al. (2009, p. 167), or other sources, the pressure drop ΔP in a fluid of density ρ flowing with velocity V along a cylindrical channel of length ΔL, vertical extent ΔZ and diameter D, is given by the continuity equation

$$\Delta P = \pm \rho g \Delta Z + \frac{f \rho V^2}{2 D} \Delta L \qquad \text{(S3.01)}$$

where f is the Darcy-Weisbach friction factor for the flow regime and g is the acceleration due to gravity. The $\pm$ sign refers to the vertical component of flow; it is + if upward and – if downward. In the limit of V=0 this equation simplifies to the standard condition for hydrostatic equilibrium; it follows (for a given pressure at the Earth's surface) that the pressure at depth in a fluid that is moving downwards will be less than if the fluid were stationary. The value of f itself depends on the Reynolds Number, Re, of the flow, where

$$Re \equiv \frac{V D \rho}{\eta} \qquad \text{(S3.02)}$$

η being the (dynamic) viscosity of the fluid. In general, if Re < ~2000, the flow is laminar, whereas at higher Re it is turbulent. For laminar flow, f takes standard values as a function of Re (e.g., McKeon et al., 2004). However, for turbulent flow, f also depends strongly on the roughness of the surface of the cylindrical channel, being markedly higher the rougher this is. Roughness, Λ, is itself defined as

$$\Lambda \equiv \frac{\varepsilon}{D}, \qquad \text{(S3.03)}$$

where ε is the characteristic height of surface irregularities. For the steel used to manufacture well casing, ε is typically ~0.016 mm (e.g., Wan, 2011, p. 131; Fekete Associates, 2013).

de Pater and Baisch (2011) reported the external diameter of the Preese Hall-1 well casing as 5.5 inches at the depths of injection. The internal diameter, D, is thus estimated as 5 inches or 127.3 mm, assuming a standard specification of casing (Hirschfeldt, 2016). It follows from equation (S3.03) that Λ was ~1.3×10^{-4} for this casing. One may look up f for this value of Λ and any given value of Re on a standard 'Moody Diagram' (Moody, 1944) for input into calculations using equation (S3.01).

To model the variation over time of the density of the material within the well, due to the injection of proppant, the distance between the wellhead and the well-casing perforations has been subdivided into ten sections of equal length. The density of the proppant entering each of these sections at each time step is assumed to apply throughout this section. No attempt has been made to model the effect of self-compression on the density of water, however. From standard theory, this effect $\Delta\rho$ for a change in pressure ΔP can be approximated as

$$\Delta\rho = \frac{\rho_o}{B} \Delta P, \qquad \text{(S3.04)}$$

where ρ_o is the initial density and B is the bulk modulus of water. Since B is large (2.15 GPa) this effect is small, amounting to 12.3 kg m^{-3} or just over 1% for a pressure increase of 26.5 MPa (corresponding to a depth increase of 2700 m; cf. Fig. 5(a)). The effect of thermal expansion of water, which (for a temperature rise to ~50 °C) will cancel the effect of self-compression, has also not been incorporated.

One expects injection of fracking fluid to be highly turbulent, to keep the proppant in suspension. Preliminary calculations assuming a representative value of η of 10^{-3} Pa s, for water at 20 °C, for representative rates of fluid injection reported by de Pater and Baisch (2011), indicate typical values for Re of ~2×10^6, confirming that the flow was indeed highly turbulent. With Re ~2×10^6 and Λ ~1.3×10^{-4}, the Moody (1944) Diagram indicates f ~0.012. However, calculations on this basis for stage 1 of the PH1 fracking result in BHP lower than the measured minimum principal stress (Fig. 6(b)), which would imply a negative net pressure, implying that that the fluid at depth was insufficiently pressurized to hold a hydraulic fracture open. Since fractures evidently developed (because fluid was injected into the rock mass surrounding the borehole) this combination of parameter values is mutually inconsistent; the data available for stage 1 indicate that f can have been no higher than ~0.01.

Heating of the fluid during injection, lowering its viscosity, might explain this inconsistency. Given the thermal conductivity of the local stratigraphy (Fig. 5(a)) and the regional heat flow (e.g., Downing and Gray, 1986; Rollin, 1995; Busby et al., 2009, 2011), ~80 °C temperatures are expected at the ~2600-2700 m depths of injection. Water is roughly one third as viscous at 80 °C compared with 20 °C (viscosity 0.355×10^{-3} Pa s at 80 °C); from equation (S3.02), Re values of ~6×10^6 might thus result. However, the Moody (1944) Diagram indicates that this would only reduce f from ~0.012 to ~0.0115. A related issue concerns the use of a friction reducer in the PH1 well; this has been reported informally, but no details have been made public. The Moody (1944) Diagram indicates that a perfectly smooth wellbore would have f ~0.0105 for Re=2×10^6 or f ~0.0087 for Re=6×10^6. The latter value is low enough to account for the pressure data; the combination of friction reducer use and heating of the injected fluid can thus account for the inconsistency, predicting a BHP high

enough to maintain a positive net pressure, sufficient to hold a fracture open, given the estimate of σ_h (using equation (3)) at the depth of injection for fracking stage 1 (Table 1).

4. Theory for hydraulic fracturing

The science of fracture mechanics was pioneered at the University of Glasgow by Sir William Rankine (e.g., Rankine, 1843, 1858). Subsequent refinements to general theory include the works of Griffith (1921, 1924), Sneddon (1951), Eshelby (1957), and Irwin (1957). Modelling of the development of hydraulic fractures has since become an extensive field, including the emergence of 'industry standard' procedures and software packages, significant contributions or syntheses including the works by Brady et al. (1992), Barree et al. (2005), Adachi et al. (2007), Rahman and Rahman (2010), Fisher and Warpinski (2012), Flewelling et al. (2013), Detournay (2016), and Ma et al. (2016).

As others (e.g., Fisher and Warpinski, 2012; Westaway and Younger, 2014) have previously discussed, the form of the ideal vertical hydraulic fracture, which develops in an isotropic medium as a consequence of horizontal minimum principal stress, will depend on the parameter K, the difference between the vertical gradient of σ_h, S, and the vertical gradient of fluid pressure (i.e.,

$$K = S - \rho g \qquad \text{(S4.01)}$$

ρ and g being, again, the density of the fluid and the acceleration due to gravity). A fracture can thus be envisaged as developing with height H between values of the vertical coordinate, y, -H/2 and +H/2, with the net pressure at y=0 designated as P_o. The form of the vertical variation in fracture width, w, in this situation was derived by Fisher and Warpinski (2012) and was analyzed further by Westaway and Younger (2014). However, rather than the rectangular fracture model investigated by Westaway and Younger (2014), the present analysis considers a variant where w tapers with an elliptical profile as a function of horizontal co-ordinate x, between x=0 at the centre-line of the fracture and x=A, its half-length, with half-length likewise tapering elliptically below a maximum at y=0.

There are, however, a number of potential reasons for departure from such idealized behaviour. First, recent investigations (e.g., Chandler et al., 2016) indicate that shales can have anisotropic mechanical properties that can affect the geometry of fracture development. For example, in the Cretaceous Mancos Shale of the western USA, the measured fracture toughness is lower for fractures developing parallel to bedding than for those with other orientations (Chandler et al., 2016). This variability will cause induced fractures to deviate away from the ideal orientation towards a more bedding-parallel orientation. If such variations in properties were to be confirmed as significant for the Bowland Shale, they would imply, given the WNW dip of the local stratigraphy (Fig. 4), that fractures might develop oriented with azimuths rotated somewhat clockwise from the 'ideal' orientation and with upward growth inclined steeply towards the ESE, rather than vertical. This aspect is noted here in passing, there currently bring no published data for the Bowland Shale on which to base an analysis that incorporates such complexity. Second, as many workers have noted, fracture development may be affected by heterogeneity within the stratigraphic column. Existing planes of weakness, such as bedding or pre-existing fractures, may accommodate the upward propagation of induced fractures by shearing. The resulting lateral steps in the induced fracture may well be impermeable, preventing the injected fluid reaching any upward tensile continuation of this induced fracture (e.g., Zhang and Li, 2016) and thus preventing it from propagating upward farther. This is different from the behaviour inferred at Preese Hall by Harper (2011), who suggested that bedding plane shear might occur but it would *increase* the permeability of the bedding-plane-parallel shear fractures and thus result in extensive leakage of fluid into these fractures. However, since the bedding at Preese Hall is inclined (e.g., Table N1; Fig. 4) it is to be expected that any induced fracture will intersect any bedding plane obliquely, rather than at a right-angle. As a result, the bedding plane will be expected to 'open' obliquely (i.e., accommodate a 'hybrid'-mode combination of tensile and shear displacement), providing an interconnection for the injected fluid between the tensile

fractures on either side. It is thus arguable that at this site the vertical growth of fractures will not be limited by this potential mechanism.

The present analysis will thus concern idealized vertical fractures, rather than the more complex geometries that might be envisaged from the above considerations. The width w of such an ideal model fracture can be written (cf. Fisher and Warpinski, 2012) as

$$w(x,y) = \frac{(1-\nu)}{2\,A\,\mu} F\,(2\,P_o + K\,y)\,\sqrt{(H^2 - 4\,y^2)}\,\sqrt{(A^2 - x^2)} \qquad \text{(S4.02)}$$

where μ and ν are the shear modulus and Poisson's ratio of the rock in which the fracture develops, A(y) is the half-length of the fracture at vertical position y, and F is a scale factor whose value will be determined below. The maximum half-length of the model fracture A(y=0) can be designated as L. The aspect ratio of this model fracture can be expressed using the parameter C, where

$$A(y=0) \equiv L \equiv C\,H\,, \qquad \text{(S4.03)}$$

so

$$A(y) \equiv C\,\sqrt{(H^2 - 4\,y^2)}\,. \qquad \text{(S4.04)}$$

The volume of this model fracture, V, can be expressed as

$$V = \int_{y=-H/2}^{y=H/2} \int_{x=-A(y)}^{x=A(y)} w(x,y)\,dx\,dy\,; \qquad \text{(S4.05)}$$

after many algebraic steps, one obtains

$$V = \frac{\pi\,(1-\nu)\,C\,F\,P_o\,H^3}{3\,\mu}\,. \qquad \text{(S4.06)}$$

As Fisher and Warpinski (2012) pointed out, the minimum net pressure condition for this model fracture to be held open is given by

$$P_o = \frac{K\,H}{4}\,. \qquad \text{(S4.07)}$$

In general, however, the pressure at y=0 might be larger than this, so this condition can be written more generally as

$$P_o = \frac{M\,K\,H}{4}\,. \qquad \text{(S4.08)}$$

where $M \geq 1$. Equation (S4.06) can therefore be rewritten using equation (S4.08) as

$$V = \frac{\pi\,(1-\nu)\,C\,F\,M\,K\,H^4}{12\,\mu}\,. \qquad \text{(S4.09)}$$

For an equidimensional (i.e., circular) model fracture of this type, for which C=1/2, one thus obtains

$$V = \frac{\pi\,(1-\nu)\,F\,M\,K\,H^4}{24\,\mu}\,. \qquad \text{(S4.10)}$$

or, using equation (S4.08) and the fact that H=2 L,

$$V = \frac{4\,\pi\,(1-\nu)\,F\,P_o\,L^3}{3\,\mu}\,. \qquad \text{(S4.11)}$$

The vertical position with the greatest width of this model fracture, along its vertical centre-line, can be found by differentiating equation (S4.02) to obtain $\partial w/\partial y$ at x=0 and solving the resulting equation for $\partial w/\partial y=0$. One thus obtains

$$y_o = \frac{-P_o}{2K} + \sqrt{\left(\frac{P_o^2}{4K^2} + \frac{H^2}{8}\right)}, \quad \text{(S4.12)}$$

or, using equation (S4.08),

$$y_o = \left[\frac{-1}{8} + \frac{1}{8}\sqrt{(M^2 + 8)}\right] H . \quad \text{(S4.13)}$$

Figure S3.1 illustrates the resulting variation of y_o/H as a function of M. It is thus evident that with M=1 (i.e., with P_o= K H/4, the minimum value at which a fracture of the required height can form; Fisher and Warpinski, 2012), y_o = H/4. Recalling that its vertical extent spans y=-H/2 to +H/2, this means that the maximum width develops three quarters of the way up the fracture. Conversely, as $M\rightarrow\infty$, $y_o/H\rightarrow 0$, meaning that the maximum width develops halfway up the fracture.

The maximum width w_o of the model fracture can be obtained as $w(x=0, y=y_o)$ from equation (S4.02). In the limit of M=1, where P_o=K H / 4 and y_o = H/4 one thus obtains

$$w_o = \frac{3\sqrt{3}\,(1-\nu)\,F\,K\,H^2}{16\,\mu}, \quad \text{(S4.14)}$$

whereas in the limit of $M\rightarrow\infty$, where $y_o\rightarrow 0$, one obtains

$$w_o = \frac{(1-\nu)\,F\,M\,K\,H^2}{4\,\mu}, \quad \text{(S4.15)}$$

giving, for an equidimensional (i.e., circular) fracture, where C=1/2 so H=2 L

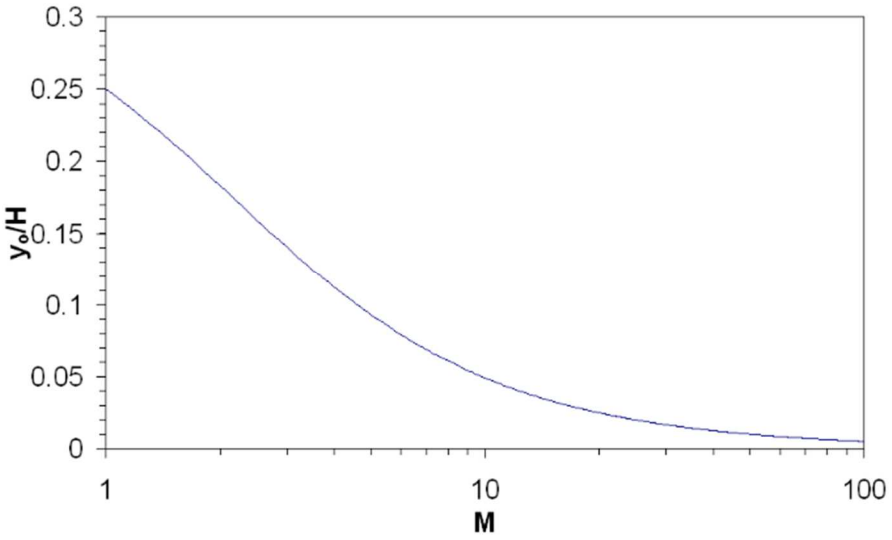

Figure S3.1. *Graph of the relation between y_o/H and M, indicated by equation (S4.13). Here, H denotes the height of a vertical fracture, M denotes the ratio of fluid pressure at y=0 to the minimum value that is able to hold open a vertical fracture of a given H, and y_o is the vertical position (relative to the mid-point of –H/2 at the lower limit and y=+H/2 at the upper limit of the fracture) at which a vertical fracture has maximum width. See text for discussion.*

$$w_o = \frac{2\,(1-\nu)\,F\,P_o\,L}{\mu}\,, \qquad \text{(S4.16)}$$

Since M can, in principle, take any value no matter how large, a fracture under significant net pressure can in principle be much wider than a fracture that forms at minimum pressure. However, since the overall volume of the fracture is limited by the fluid available to hold it open (e.g., Fisher and Warpinski, 2012), it follows that a fracture under significant net pressure will be smaller (in terms of H and/or L) than one formed by injection of the same volume of fluid under minimum pressure conditions.

The equidimensional (i.e., circular) case in the limit of $M\rightarrow\infty$ (such that vertical variations in pressure are small compared with the overall excess pressure) is equivalent to the classical problem of a circular fracture of radius A under uniform net pressure, which was solved by Sneddon (1951; equation 128 on p. 490). As Westaway and Younger (2014) and Westaway (2015a) have discussed, this solution can be written using the present notation as

$$w(r) = \frac{4\,(1-\nu)\,P_o}{\pi\,\mu}\sqrt{(L^2 - r^2)}\,, \qquad \text{(S4.17)}$$

r being the distance from the centre of the fracture and L being the radius of the fracture, giving

$$w_o \equiv w(r=0) = \frac{4\,(1-\nu)\,P_o\,L}{\pi\,\mu}\,, \qquad \text{(S4.18)}$$

and

$$V = \frac{8\,(1-\nu)}{3\,\mu}\,P_o\,L^3\,. \qquad \text{(S4.19)}$$

Comparison of equations (S4.16) and (S4.18), or (S4.11) and (S4.19), indicates that $F=2/\pi$. Thus, for example, for an equidimensional (i.e., circular) model fracture of this type at minimum pressure one obtains

$$w_o = \frac{3\sqrt{3}\,(1-\nu)\,K\,H^2}{8\,\pi\,\mu}\,, \qquad \text{(S4.20)}$$

or

$$w_o = \frac{3\sqrt{3}\,(1-\nu)\,K\,L^2}{2\,\pi\,\mu}\,, \qquad \text{(S4.21)}$$

or

$$w_o = \frac{3\sqrt{3}\,(1-\nu)\,P_o\,L}{\pi\,\mu}\,, \qquad \text{(S4.22)}$$

with, once again,

$$V = \frac{8\,(1-\nu)\,P_o\,L^3}{3\,\mu}\,. \qquad \text{(S4.23)}$$

or

$$V = \frac{4\,(1-\nu)\,K\,L^4}{3\,\mu}\,. \qquad \text{(S4.24)}$$

For comparison, the equidimensional (i.e., square) variant of the Westaway and Younger (2014) rectangular fracture model of half-length L, at minimum pressure, specifies

$$w_o = \frac{3\sqrt{3}\,(1-\nu)\,K\,L^2}{4\,\mu}, \quad \text{(S4.25)}$$

or

$$w_o = \frac{3\sqrt{3}\,(1-\nu)\,P_o\,L}{2\,\mu}, \quad \text{(S4.26)}$$

(from their equation (A28)), and

$$V = \frac{\pi\,(1-\nu)\,K\,L^4}{\mu}. \quad \text{(S4.27)}$$

or

$$V = \frac{2\,\pi\,(1-\nu)\,P_o\,L^3}{\mu}. \quad \text{(S4.28)}$$

(from their equation (A32)). For a given set of parameter values, the dimensions of the two models are comparable. Thus, for example, for the same K and L, the circular model has $2/\pi$ or ~0.637 of the maximum width and $4/(3\,\pi)$ or ~0.424 of the volume of the square model. For the same K and V, the circular model has $(3\,\pi\,/\,4)^{1/4}$ or ~1.239 times the height and width of the square model. For the same P_o and V, the circular model has $(3\,\pi\,/\,4)^{1/3}$ or ~1.331 times the height and width of the square model. These modest differences are to be expected given that the square model fracture is open in its 'corners' whereas the circular variant is not.

The aspect ratio C for the induced fracture is not directly specified by the present model and requires separate determination. As many workers have noted, in rheologically-stratified sediments fractures can be 'confined' within shale layers and can thus develop substantial lengths with limited heights, with C>>1; however, one does not expect such behaviour within a relatively homogenous succession such as the Bowland Shale. A potential criterion for constraining C can be derived from consideration of the stress intensity, K_I, during fracturing:

$$K_I = \sigma\,\sqrt{(\pi\,\lambda)}\,, \quad \text{(S4.29)}$$

where σ is the stress tensor element driving the fracture and λ is the length of the fracture in the direction of propagation. Irwin's (1957) work introduced the notion that fractures propagate when K_I reaches or exceeds a critical value, known as the fracture toughness. Assuming that vertical and horizontal fracture growth occur concurrently in the same lithology, both will therefore cease when K_I falls below the fracture toughness. Thus, for a fracture under significant net pressure, σ will approximate the same value, P_o, at all points along the fracture front so λ will be expected to be the same in all directions if K_I is isotropic, making the fracture equidimensional (i.e., C=1/2). Conversely, under minimum pressure conditions, σ will equal $2\,P_o$ at the top of the fracture, for which λ =H, and will equal P_o at its horizontal extremities, which (as noted above; equation (S4.03)) occur halfway up the fracture, where $\lambda = 2\,L$. Equating the versions of equation (S4.29) for these two points on the fracture front, again assuming that K_I is isotropic, gives

$$2\,P_o\,\sqrt{(\pi\,H)} = P_o\,\sqrt{(2\,\pi\,L)}. \quad \text{(S4.30)}$$

or

$$L = 2\,H\,, \quad \text{(S4.31)}$$

so, from equation (S4.03), C=2. Under these minimum-pressure conditions, the model fracture is thus predicted to develop elliptical form, with its length four times its height.

As already noted, Chandler et al. (2016) have argued on the basis of the Mancos Shale that fracture toughness in shale is not isotropic. However, their measurements indicate that fracture toughness does not differ significantly for a fracture developing in 'arrester' mode (corresponding to the upward component of growth of a fracture developing in a vertical plane in response to anisotropic properties determined by horizontal bedding) compared with one developing in 'divider' mode (corresponding to the horizontal component of growth of a fracture developing in a vertical plane in response to anisotropic properties determined by horizontal bedding).

In summary, the above considerations collectively determine the form of the model fracture, points on whose elliptical perimeter have coordinates (x,y) that satisfy the equations

$$x = L \cos(\theta) \qquad \text{(S4.32)}$$

and

$$y = y_m + \frac{H \sin(\theta)}{2}, \qquad \text{(S4.33)}$$

where θ varies between 0 and 360°, and y_m (the vertical midpoint of the fracture), L and H are determined using the preceding equations.

The above considerations bear upon the potential for vertical growth of hydraulic fractures to cause environmental pollution, as a result of breaching upward into sediments that are used for water supply (e.g., Fisher and Warpinski, 2012; Davies et al., 2013; Westaway and Younger, 2014; Younger, 2016a). It is evident that if such a breach were to occur then, rather than pollution entering shallower groundwater zones, the result would be for shallower groundwater to flood downward into the fracture, preventing shale gas production, so shale operators have a strong incentive to ensure that this does not happen (e.g., Westaway and Younger, 2014; Younger, 2016b). Nonetheless, the calculations indicate that under minimum pressure conditions the induced fracture height is proportional to the fourth root of the injected volume, whereas at high net pressure it is proportional to the cube root of the injected volume. Moreover, the above suggestion that minimum-pressure conditions will create induced fractures with aspect ratios >1 will further mitigate height growth. Westaway and Younger (2014) recognized this fourth-root dependence for their square and rectangular fracture models under minimum-pressure conditions; it is now apparent that such dependence has wider applicability. Conversely, others (e.g., Flewelling et al., 2013) have previously noted cube root dependence between injected volume and induced fracture height, without realising that this is not always valid; as discussed above, it requires the effect of the vertical gradient in excess pressure to be negligible, so (under real conditions where this gradient is nonzero) will only apply where the net pressure is large compared with the difference in pressure between the top and bottom of the fracture.

5. Theory for Coulomb failure analysis

The Coulomb failure criterion will be used in the present analysis to assess whether the condition for shear failure is satisfied at a given point on a fault or within an unfractured rock mass, like in many previous analyses (e.g., those by Westaway, 2002, 2006, 2015a). The parameter Φ will thus be evaluated:

$$\Phi = \tau - c\,(\sigma_n - P_f) - S_C\,, \qquad \text{(S5.01)}$$

where σ_n, τ and c are the resolved normal stress, shear stress and coefficient of friction on the fault plane (or coefficient of internal friction within the rock mass), and P_f and S_C are the pore-fluid pressure and cohesion of the fault zone or rock mass. Φ=0 marks this condition, with Φ<0 indicating stability at the point analyzed under the current state of stress. In general, this condition for shear failure can also be visualized graphically using the standard Mohr circle construction (Fig. S4.1).

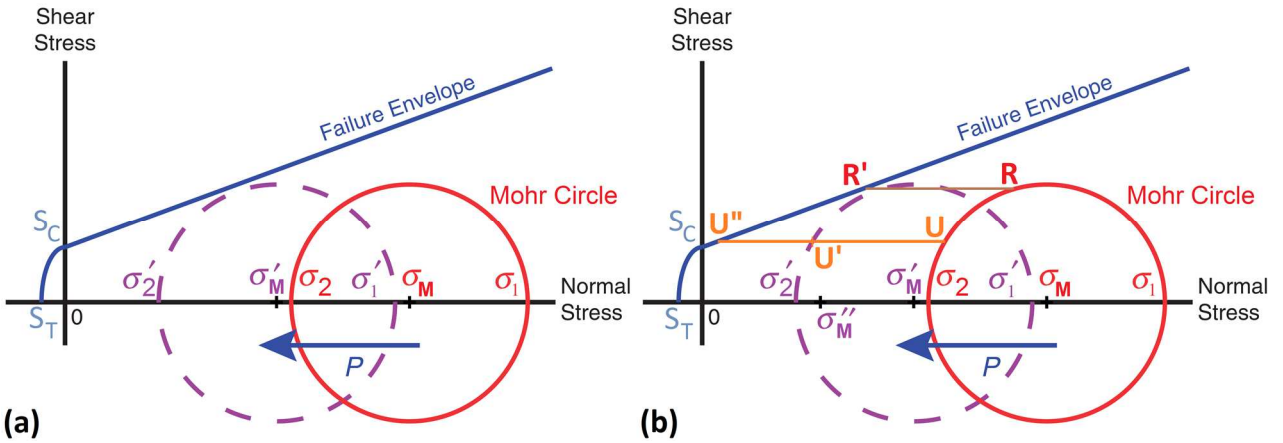

Figure S4.1. *Schematic illustration of the physical mechanism whereby fluid injection can cause induced seismicity, using a Mohr Circle / Failure Envelope representation of stress state. Normal stress (compressional when positive and tensile when negative) is plotted on the horizontal axis, with shear stress on the vertical axis. The maximum and minimum normal stresses acting at a given locality are plotted as σ_1 and σ_2; these lie at opposite ends of a diameter of a circle that is centred at the point on the horizontal axis where the normal stress equals the mean stress σ_M (where $\sigma_M = (\sigma_1 + \sigma_2)/2$) and has radius $\Delta\sigma/2$ where $\Delta\sigma = \sigma_1 - \sigma_2$ is the differential stress. This Mohr Circle represents the set of combinations of normal and shear stress that act in different directions at the locality. The failure envelope represents the set of combinations of normal and shear stress that result in rock failing in shear or in tension, or a pre-existing fault or tensile fracture being reactivated. Its gradient equals the coefficient of friction of a pre-existing fault, or the coefficient of internal friction within a rock mass, c. This envelope passes through a point on the horizontal axis where the tensile normal stress equals the tensile strength S_T of the material, and a point on the vertical axis where the shear stress equals its cohesion S_C. Intact rock will have nonzero S_C and S_T; as discussed by Westaway and Younger (2014), pre-existing faults or fractures in some rocks, such as shale, might likewise have nonzero S_C and S_T, so this possibility is allowed for here. (a) 'Conventional' usage of this method for a permeable rock in which interconnected pore fluid occupies the matrix and its pressure P acts in all directions. When fluid pressure is increased by P, the mean stress decreases from σ_M to $\sigma'_M = \sigma_M - P$ and the Mohr Circle effectively shifts leftward by a distance P (to the dashed circle depicted), resulting in new 'effective' maximum and minimum normal stresses $\sigma'_1 = \sigma_1 - P$ and $\sigma'_2 = \sigma_2 - P$. This normal-stress reduction has the consequence of bringing any fault nearer to the condition for slip, regardless of its orientation, as can be visualized from the closer proximity of all points on the dashed Mohr Circle to the failure envelope. If the pressure increase is large enough such that any point on the adjusted Mohr Circle touches the failure envelope, the fault will slip (or the rock will fail to create a new fault with the orientation indicated) and an induced earthquake will result. The orientation of the failure plane (in Mohr circle space) is that of the normal to the failure envelope at the point where it touches the Mohr circle. (b) Revision to deal with impermeable rocks (cf. Hackston and Rutter, 2016; Rutter and Hackston, in review), in which pore fluid is absent from any matrix and is only present in pre-existing faults and fractures, such that its pressure only acts in the directions perpendicular to the plane of the fault or fracture. Suppose U denotes the orientation (in Mohr circle space) of a pre-existing fault or fracture. The pressure increase within this structure, by P, will displace it in Mohr circle space to U'; since this point lies below the failure envelope, no failure will occur. This is even though the corresponding increase in P displaces another point on the Mohr circle (R, which does not correspond to any pre-existing fault or fracture) to point R', which does lie on the failure envelope. To cause failure on structure U, a much larger pressure increase would be necessary, to displace U to U'' on the failure envelope. At this stage the mean stress would be σ''_M and the orientation of the failure in Mohr circle space would be given by U''-σ''_M which is equivalent to U-σ_M. The orientation of this failure would, therefore, not correspond to that of the normal to the failure envelope. Much of the 'displaced' Mohr circle would lie above this failure envelope but the parts of it that do not correspond to orientations of pre-existing faults or fractures have no meaning in this context and thus provide no indication of the orientation at which failure will occur. When using the Mohr circle construction in this context it is thus preferable to omit the 'displaced' Mohr circle and to only show in Mohr circle space 'displaced' points that correspond to orientations of faults or fractures, as is done in Fig. 8 in the main text. Alternatively, since, in this context of impermeable rocks, failure can only occur on pre-existing structures (unless, of course, the increase in fluid pressure takes the state of stress into the tensile domain), one does not need to use the Mohr circle construction to test whether other orientations might fail preferentially; one can thus solve such problems straightforwardly using vector geometry, as is done in the present text. Modified from Figure 1 of Westaway (2015a), based on Fig. 3 of Rubinstein and Mahani (2015).*

Once the condition Φ=0 occurs and an earthquake results, the state of stress will change across the model, with the patch of fault that slipped becoming de-stressed and an adjoining region of similar dimensions becoming more highly stressed (e.g., Stein et al., 1996, 1997). For rupture of a circular patch of fault, the stress drop $\Delta\sigma$ is given by

$$\Delta\sigma = \frac{3\,(2 - \nu)\,\pi}{16\,(1 - \nu)}\,\mu\,k\,. \qquad \text{(S5.02)}$$

(Westaway and Younger, 2014), where k is the ratio of maximum slip to fault radius. Typically, k is observed to be ~10^{-4} to ~10^{-5}; for the larger of these values, and with μ=10 GPa and ν=0.15, $\Delta\sigma$ is thus ~1.3 MPa. Conversely, regions adjoining patches of fault that slip can become more highly stressed by up to ~1 MPa (e.g., Stein et al., 1996, 1997).

To calculate Φ at points on a model fault, given the stress tensor σ with elements σ_{ij} at each point, the following technique (consistent with standard theory; e.g., Ciarlet, 1988; Jaeger et al., 2007, p. 31) has been used. The unit normal vector **n** to the fault, with components n_i, was determined, thus giving the Cauchy stress vector **T** where, using the standard summation notation,

$$T_j = \sigma_{ij}\,n_j\,. \qquad \text{(S5.03)}$$

The normal stress was thus determined as

$$\sigma_n = T_i\,n_i = \sigma_{ij}\,n_j\,n_j\,, \qquad \text{(S5.04)}$$

the corresponding shear stress τ then being found using the standard formula

$$\tau = \sqrt{(T_i\,T_i - \sigma_n^2)}. \qquad \text{(S5.05)}$$

To calculate the corresponding angles for the analysis of the stress state, I note that vector **B** where

$$\mathbf{B} = \mathbf{n} \times \mathbf{T} \quad (\text{or } B_i = \varepsilon_{ijk}\,n_j\,T_k) \qquad \text{(S5.06)}$$

(vectors **n** and **T** having been defined earlier) is oriented along the null axis and vector **U** where

$$\mathbf{U} = \mathbf{n} \times \mathbf{B} \quad (\text{or } U_i = \varepsilon_{ijk}\,n_j\,B_k) \qquad \text{(S5.07)}$$

is oriented along the direction of slip. The $\times$ symbol in these equations denotes the vector product operation; in the alternative notation, ε_{ijk} is the antisymmetric permutation symbol or Levi-Civita symbol.

References

Adachi, J., Siebrits, E., Peirce, A., Desroches, J., 2007. Computer simulation of hydraulic fractures. International Journal of Rock Mechanics & Mining Sciences, 44, 739–757.

Andrews, I.J., 2013. The Carboniferous Bowland Shale gas study: geology and resource estimation. British Geological Survey for Department of Energy and Climate Change, London, 64 pp.

Baisch, S., Vörös, R., 2011. Geomechanical study of Blackpool seismicity. Report for Cuadrilla Resources, 58 pp. Available online: http://www.cuadrillaresources.com/wp-content/uploads/2012/02/Geomechanical-Study-Appendix-2-2.11.2011.pdf (accessed 30 November 2016)

Baker Hughes, 2011. Wellbore failure analysis and geomechanical modelling in the Bowland Shales, Blackpool, UK: preliminary technical report. Baker Hughes Incorporated, Houston, Texas, 53 pp. Available online: http://www.cuadrillaresources.com/wp-content/uploads/2012/02/Geomechanical-Study-Appendix-1-2.11.2011.pdf (accessed 10 May 2015)

Baptie, B., 2010. Seismogenesis and state of stress in the UK. Tectonophysics, 482, 150–159.

Barree, R.D., Cox, S.A., Gilbert, J.V., Dobson, M.L., 2005. Closing the gap: fracture half length from design, buildup, and production analysis. Society of Petroleum Engineers document SPE-84491-PA. SPE Production & Facilities, 20 (4), 12 pp. doi: http://dx.doi.org/10.2118/84491-PA

Bott, M.H.P., 1988. The Market Weighton gravity anomaly — granite or graben? Proceedings of the Yorkshire Geological Society, 47, 47-53.

Bott, M.H.P., Robinson, J., Kohnstamm, M.A., 1978. Granite beneath Market Weighton, east Yorkshire. Journal of the Geological Society, London, 135, 535-543.

Brady, B., Elbel, J., Mack, M., Morales, H., Nolte, K., Poe, B., 1992. Cracking rock: progress in fracture treatment design. Oilfield Review, October 1992, 4-17.

Bridgland, D.R., Westaway, R., Howard, A.J., Innes, J.B., Long, A.J., Mitchell, W.A., White, M.J., White, T.S., 2010. The role of glacio-isostasy in the formation of post-glacial river terraces in relation to the MIS 2 ice limit: evidence from northern England. Proceedings of the Geologists' Association, 121, 113-127.

Bridgland, D.R., White, T.S., Howard, A.J., White, M.J., Westaway, R., 2014. Chapter 6. Synthesis: the Pleistocene evolution and human occupation of the Trent catchment. In: Bridgland, D.R., Howard, A.J., White, M.J., White, T.S. (eds), The Quaternary of the Trent. Oxbow Books, Oxford, pp. 295-372.

British Coal Corporation, 1997. Three-dimensional seismic surveying to investigate the geological structure of shear zones within the Selby coalfield. European Union, Directorate-General Energy, report EUR 17161 EN. Office for Official Publications of the European Communities, Luxembourg, 122 pp.

Browning, G.R.J., Jacob, A.W.B., 1970. Preliminary study of the North of England earthquake of August 9, 1970. Nature, 228, 835-837.

Busby, J., Lewis, M., Reeves, H., Lawley, R., 2009. Initial geological considerations before installing ground source heat pump systems Quarterly Journal of Engineering Geology and Hydrogeology, 42, 295-306.

Busby, J., Kingdon, A., Williams, J., 2011. The measured shallow temperature field in Britain. Quarterly Journal of Engineering Geology and Hydrogeology, 44, 373-387.

Carter, P.G., Mills, D.A., 1976. Engineering geological investigations for the Kielder Tunnels. Quarterly Journal of Engineering Geology and Hydrogeology, 9, 125-141.

Cartwright, P.B., 1997. A review of recent in-situ stress measurements in United Kingdom Coal Measures strata. In: Sugawara, K., Obara, Y. (eds), Rock Stress: Proceedings of the International Symposium on Rock Stress, Kumamoto, Japan, 7-10 October 1997. Balkema, Rotterdam, pp. 469-474.

Chadwick, R.A., Holliday, D.W., Holloway, S., Hulbert, A.G., 1995. The structure and evolution of the Northumberland-Solway Basin and adjacent areas. British Geological Survey Subsurface Memoir. HMSO, London, 90 pp.

Chadwick, R.A., Pharaoh, T.C., Williamson, J.P., Musson, R.M.W., 1996. Seismotectonics of the UK. British Geological Survey Technical Report, WA/96/3C. British Geological Survey, Keyworth, Nottingham, 172 pp. Available online: http://core.ac.uk/download/pdf/59774.pdf (accessed 16 October 2015)

Chandler, M.R., Meredith, P.G., Brantut, N., Crawford, B.R., 2016. Fracture toughness anisotropy in shale. Journal of Geophysical Research, Solid Earth, 121, 1706–1729, doi: 10.1002/2015JB012756.

Ciarlet, P.G., 1988. Mathematical Elasticity: Three-dimensional elasticity, Volume 1. Elsevier, Amsterdam, 455 pp.

Clarke, H., 2016. Reply to “Hydraulic fracturing in thick shale basins: problems in identifying faults in the Bowland and Weald Basins, UK” by D.K. Smythe. Interactive Discussion item SC9, 7 pp. Available online: http://www.solid-earth-discuss.net/se-2015-134/discussion (accessed 3 March 2016)

Clarke, H., Eisner, L., Styles, P., Turner, P., 2014. Felt seismicity associated with shale gas hydraulic fracturing: The first documented example in Europe. Geophysical Research Letters, 41, 8308–8314.

Cuadrilla, 2014. Temporary Shale Gas Exploration; Preston New Road, Lancashire; Environmental Statement, Appendix L – Induced Seismicity. Cuadrilla Bowland Ltd., Lichfield. 140 pp. Available online: http://planningregister.lancashire.gov.uk/Attachments/6586/PNR_ES_Vol2_Appndx_L_Induced Seismicity.pdf (accessed 9 March 2015).

Davies, R., Foulger, G., Bindley, A., Styles, P., 2013. Induced seismicity and hydraulic fracturing for the recovery of hydrocarbons. Marine and Petroleum Geology, 45, 171-185.

de Paola, N., Holdsworth, R.E., McCaffrey, K.J.W., 2005. The influence of lithology and pre-existing structures on reservoir-scale faulting patterns in transtensional rift zones. Journal of the Geological Society, London, 162, 471–480.

de Pater, C.J., Baisch, S., 2011. Geomechanical study of Bowland Shale seismicity: synthesis report. Cuadrilla Resources Ltd., Lichfield, 71 pp. Available online: http://www.rijksoverheid.nl/bestanden/documenten-en-publicaties/rapporten/2011/11/04/rapport-geomechanical-study-of-bowland-shale-seismicity/rapport-geomechanical-study-of-bowland-shale-seismicity.pdf (accessed 5 August 2015)

Detournay, E., 2016. Mechanics of hydraulic fractures. Annual Review of Fluid Mechanics, 48, 311–339.

Downing, R.A., Gray, D.A. (eds), 1986. Geothermal Energy - The Potential in the United Kingdom. Her Majesty's Stationery Office, London, 187 pp.

Dunham, K.C., 1974. Granite beneath the Pennines in North Yorkshire. Proceedings of the Yorkshire Geological Society, 40, 191-194.

Dunham, K.C., Wilson, A.A., 1985. Geology of the Northern Pennine Orefield; Volume 2, Stainmore to Craven. Economic Memoir of the British Geological Survey, England and Wales, Sheets 40, 41, and 50 and parts of 31, 32, 51, 60 and 61.

Eshelby, J.D., 1957. The determination of the elastic field of an ellipsoidal inclusion, and related problems. Proceedings of the Royal Society of London, Series A, 241, 376-396.

Evans, C.J., Brereton, N.R., 1990. In situ crustal stress in the United Kingdom from borehole breakouts. In: Hurst, A., Lovell, M.A., Morton, A.C. (eds), Geological Applications of Wireline Logs. Geological Society, London, Special Publications, 48, 327-338.

Fekete Associates, 2013. Wellbore Configuration. IHS, Inc., Houston, Texas. Available online: http://www.fekete.com/SAN/WebHelp/virtuwell/webhelp/c-sw-wellbore.htm (accessed 7 August 2016)

Ferrill, D.A., Morris, A.P., Smart, K.J., 2007. Stratigraphic control on extensional fault propagation folding: Big Brushy Canyon monocline, Sierra Del Carmen, Texas. In: Jolley, S.J., Barr, D., Walsh, J.J., Knipe, R.J. (eds), Structurally Complex Reservoirs. Geological Society, London, Special Publications, 292, 203-217.

Fisher, K., Warpinski, N., 2012. Hydraulic-fracture-height growth: Real data. Society of Petroleum Engineers, Productions and Operations Journal, 27, 8–19.

Flewelling, S.A., Tymchak, M.P., Warpinski, N., 2013. Hydraulic fracture height limits and fault interactions in tight oil and gas formations. Geophysical Research Letters, 40, 3602–3606.

Fraser, A.J., Gawthorpe, R.L., 2003. An atlas of Carboniferous basin evolution in northern England. Geological Society, London, Memoir 28, 79 pp.

Fraser, A.J., Nash, A.J., Steele, R.P., Ebdon, C.C., 1990. A regional assessment of the intra-Carboniferous play of northern England. In: Brooks, J. (ed.), Classic Petroleum Provinces. Geological Society, London, Special Publications, 50, 417-440.

Froidevaux, C., Paquin, C., Souriau, M., 1980. Tectonic stresses in France: in situ measurements with a flat jack. Journal of Geophysical Research, 85, 6342-6346.

Gao Quan, Tao JunLiang, Hu JianYing, Yu Xiong, 2015. Laboratory study on the mechanical behaviors of an anisotropic shale rock. Journal of Rock Mechanics and Geotechnical Engineering, 7, 213–219.

Gawthorpe, R.L., Clemmey, H., 1985. Geometry of submarine slides in the Bowland Basin (Dinantian) and their relation to debris flows. Journal of the Geological Society, London, 142, 555-565.

GFZ, 2015. Download the World Stress Map database Release 2008. http://dc-app3-14.gfz-potsdam.de/pub/stress_data/stress_data_frame.html (accessed 10 May 2015)

Griffith, A.A., 1921. The phenomena of rupture and flow in solids. Philosophical Transactions of the Royal Society of London, Series A, 221, 163–198.

Griffith, A.A., 1924. The theory of rupture. In: Biezeno, C.B., Burgers, J.M. (eds), Proceedings of the First International Congress of Applied Mechanics, Delft, The Netherlands. Technische Boekhandel en Drukkerij, Delft, The Netherlands, pp. 55–63.

Hackston, A., Rutter, E., 2016. The Mohr–Coulomb criterion for intact rock strength and friction – a re-evaluation and consideration of failure under polyaxial stresses. Solid Earth, 7, 493–508. doi: 10.5194/se-7-493-2016

Harding, P., Bridgland, D.R., Allen, P., Bradley, P., Grant, M.J, Peat, D., Schwenninger, J.-L., Scott, R., Westaway, R., White, T.S., 2012 Chronology of the Lower and Middle Palaeolithic in NW Europe: developer-funded investigations at Dunbridge, Hampshire, southern England. Proceedings of the Geologists' Association, 123, 584-607.

Harper, T.R., 2011. Well Preese Hall-1: The mechanism of induced seismicity. Geosphere Ltd., Beaworthy, Devon, 67 pp. Available online: http://www.cuadrillaresources.com/wp-content/uploads/2012/06/Geosphere-Final-Report.pdf (accessed 17 October 2015)

Heidbach, O., Tingay, M., Barth, A., Reinecker, J., Kurfeß, D., Müller, B., 2010. Global crustal stress pattern based on the World Stress Map database release 2008. Tectonophysics, 482, 3-15.

Hills, E.S., 1966. Elements of Structural Geology. Methuen, London, 483 pp.

Hirschfeldt, M., 2016. API casing table specification. Available online: http://www.oilproduction.net/files/002-apicasing.pdf (accessed 7 August 2016)

iGas, 2014. Executive summary of Barton Moss well results. iGas Energy plc, London, 6 pp. Available online: www.igasplc.com/media/10895/barton-moss-results.pdf (accessed 1 December 2016)

Irwin, G., 1957. Analysis of stresses and strains near the end of a crack traversing a plate. Journal of Applied Mechanics, 24, 361–364.

Jaeger, J.C., Cook, N.G.W., Zimmerman, R., 2007. Fundamentals of rock mechanics, 4th edition. Blackwell, Oxford, 475 pp.

Kimbell, G.S., Young, B., Millward, D., Crowley, Q.G., 2010. The North Pennine batholith (Weardale Granite) of northern England: new data on its age and form. Proceedings of the Yorkshire Geological Society, 58, 107-128.

King, D., Browne, J., Layard, R., O'Donnell, G., Rees, M., Stern, N., Turner, A., 2015. A Global Apollo Programme to Combat Climate Change. Centre for Economic Performance, London School of Economics and Political Science, 40 pp. Available online: http://cep.lse.ac.uk/pubs/download/special/Global_Apollo_Programme_Report.pdf (accessed 9 October 2015)

Kingdon, A., Fellgett, M.W., Williams, J.D.O., 2016. Use of borehole imaging to improve understanding of the in-situ stress orientation of Central and Northern England and its implications for unconventional hydrocarbon resources. Marine and Petroleum Geology, 73, 1-20.

Kirby, G.A., Baily, H.E., Chadwick, R.A., Evans, D.J., Holliday, D.W., Holloway, S., Hulbert, A.G., Pharaoh, T.C., Smith, N.J.P., Aitkenhead, N., Birch, B. 2000. The structure and evolution of the Craven Basin and adjacent areas. Subsurface Memoir of the British Geological Survey.

Lyons, W.C., Go BoYun, Graham, R.L., Hawley, G.D., 2009. Air and Gas Drilling Manual: Applications for Oil and Gas Recovery Wells and Geothermal Fluids Recovery Wells. Elsevier, Amsterdam.

Ma Shou, Guo JianChun, Li LianChong, Xia YingJie, Yang Tao, 2016. Experimental and numerical study on fracture propagation near open-hole horizontal well under hydraulic pressure. European Journal of Environmental and Civil Engineering, 20, 412–430.

McKenzie, D.P., 1969. The relationship between fault plane solutions for earthquakes and the directions of the principal stresses. Bulletin of the Seismological Society of America, 59, 591-601.

McKeon, B.J., Swanson, C.J., Zagarola, M.V., Donnelly, R.J., Smits, A.J., 2004. Friction factors for smooth pipe flow. Journal of Fluid Mechanics, 511, 41–44.

Mark, C., Gadde, M., 2008. Global trends in coal mine horizontal stress measurements. In: Peng, S.S., Tadolini, S.C., Mark, C., Finfinger, G.L., Heasley, K.A., Khair, A.W., Luo, Y. (eds), Proceedings of the 27th International Conference on Ground Control in Mining. West Virginia University Press, Morgantown, West Virginia, pp. 319-331.

Millward, D., 2006. Caledonian intrusive rocks of northern England and the Midlands. In: Brenchley, P.J., Rawson, P.F. (eds), The Geology of England and Wales, 2nd edition. The Geological Society, London, pp. 147-154.

Moody, L.F., 1944. Friction factors for pipe flow. Transactions of the American Society of Mechanical Engineers, 66, 671–684.

Musson, R.M.W., 2007. British earthquakes. Proceedings of the Geologists' Association, 118, 305-337.

Parker, R., 1999. The Rosemanowes HDR project 1983-1991. Geothermics, 28, 603-615.
Pharaoh, T.C., Allsop, J.M., Holliday, D.W., Merriman, R.J., Kimbell, G.S., Rundle, C.C., Brewer, T.S., Noble, S.R., Evans, C.J., 1997. The Moorby Microgranite: a deformed high level intrusion of Ordovician age in the concealed Caledonian basement of Lincolnshire. Proceedings of the Yorkshire Geological Society, 51, 329–342.
Pharaoh, T.C., Vincent, C., Bentham, M.S., Hulbert, A.G., Waters, C.N., Smith, N.J.P., 2011. Structure and evolution of the East Midlands region of the Pennine Basin. Subsurface Memoir of the British Geological Survey. British Geological Survey, Nottingham, 144 pp.
Pine, R.J., Batchelor, A.S., 1984. Downward migration of shearing in jointed rock during hydraulic injections. International Journal of Rock Mechanics and Mining Sciences & Geomechanics Abstracts, 21 (5), 249-263.
Rahman, M.M., Rahman, M.K., 2010. A review of hydraulic fracture models and development of an improved pseudo-3d model for stimulating tight oil/gas sand. Energy Sources, Part A, 32, 1416–1436.
Rankine, W.J.M., 1843. On the causes of the unexpected breakage of the journals of railway axles, and on the means of preventing such accidents by observing the law of continuity in their construction. Minutes of the Proceedings of the Institution of Civil Engineers, 2, 105-107.
Rankine, W.J.M., 1858. A Manual of Applied Mechanics. Richard Griffin and Company, Glasgow, 640 pp.
Richards, H.G., Parker, R.H., Green, A.S.P., Jones, R.H., Nicholls, J.D.M., Nicol, D.A.C., Randall, M.M., Richards, S., Stewart, R.C., Willis-Richards, J., 1994. The performance and characteristics of the experimental hot dry rock geothermal reservoir at Rosemanowes, Cornwall (1985–1988). Geothermics, 23, 73-109.
Richardson, R.M., Solomon, S.C., Sleep, N.H., 1979. Tectonic stress in the plates. Reviews of Geophysics and Space Physics, 17, 981-1019.
Ringrose, P.S., 1989. Recent fault movement and palaeoseismicity in western Scotland. Tectonophysics, 163, 315-321.
Robson, D.A., 1964. The Acklington Dyke – a proton magnetometer survey. Proceedings of the Yorkshire Geological Society, 34, 293-308.
Robson, D.A., 1977. The structural history of the Cheviot and adjacent regions. Scottish Journal of Geology, 13, 255-262.
Roche, V., Grob, M., Eyre, T., Van Der Baan, M., 2015. Statistical characteristics of microseismic events and in-situ stress in the Horn River Basin. In: Proceedings of GeoConvention 2015, Calgary, Canada, 4-8 May 2015, 5 pp. Available online: http://www.geoconvention.com/uploads/2015abstracts/080_GC2015_Statistical_characteristics_of_microseismic_events.pdf (accessed 11 May 2015)
Rollin, K.E., 1995. A simple heat-flow quality function and appraisal of heat-flow measurements and heat-flow estimates from the UK Geothermal Catalogue. Tectonophysics, 244, 185–196.
Rowland, J.P., 1933. Wensleydale earthquake. Nature, 131, 128.
Rubinstein, J.L., Mahani, A.B., 2015. Myths and facts on waste water injection, hydraulic fracturing, enhanced oil recovery, and induced seismicity. Seismological Research Letters, 86, 1060-1067.
Rutter, E.H., Hackston, A., in review. On the effective stress law for rock-on-rock frictional sliding, and fault slip triggered by means of fluid injection
Rutter, E.H., Mecklenburgh, J., 2017. Hydraulic conductivity of bedding-parallel cracks in shale as a function of shear and normal stress. In: Rutter, E.H., Mecklenburgh, J., Taylor, K.G. (eds), Geomechanical and Petrophysical Properties of Mudrocks. Geological Society, London, Special Publications, 454, http://doi.org/10.1144/SP454.
Sneddon, I.N., 1951. Fourier Transforms. McGraw-Hill, New York, 542 pp.
Stein, R.S., Barka, A.A., Dieterich, J.H., 1997. Progressive failure on the North Anatolian fault since 1939 by earthquake stress triggering. Geophysical Journal International, 128, 594-604.
Stein, R.S., Dieterich, J.H., Barka, A.A., 1996. Role of stress triggering in earthquake migration on the North Anatolian Fault. Physics and Chemistry of the Earth, 21, 225-230.
Stewart, I., Firth, C., Rust, D., Collins, P., Firth, J., 2001. Postglacial fault movement and palaeoseismicity in western Scotland: a reappraisal of the Kinloch Hourn fault, Kintail. Journal of Seismology, 5, 307-328.
Sylvester, A.G., 1988. Strike-slip faults. GSA Bulletin, 100, 1666-1703.

Turner, B.R., Robson, D.A., Dearman, W.R., Jones, J.M., Magraw, D., Smith, F.W., 1995. Structure. In: Johnson, G.A.L. (ed.), Robson's Geology of North East England, 2nd edition. Transactions of the Natural History Society of Northumbria, 56, 331-343.

Versey, H.C., 1939. The North Sea earthquake of 1931 June 7. Monthly Notices of the Royal Astronomical Society, Geophysical Supplement, 4 (6), 416–423.

Versey, H.C. 1948. The Skipton earthquake of 1944. Transactions of the Leeds Geological. Association 6, 95-97.

Versey, H.C., 1949. Skipton earthquake of 1944. Nature, 163, 596.

Wan RenPu, 2011. Advanced Well Completion Engineering, 3rd Edition. Elsevier, Amsterdam, 715 pp.

Waters, C.N., Davies, S.J., 2006. Carboniferous: extensional basins, advancing deltas and coal swamps. In: Brenchley, P.J., Rawson, P.F. (eds), The Geology of England and Wales, 2nd edition. The Geological Society, London, pp. 173-223.

Waters, C.N., Somerville, I.D., Jones, N.S., and 16 others, 2011. A revised correlation of Carboniferous Rocks in the British Isles. Geological Society, London, Special Report 26.

Waters, C.N., Glover, B.W., Powell, J.H., 1994. Structural synthesis of south Staffordshire, UK: implications for the Variscan evolution of the Pennine Basin. Journal of the Geological Society, London, 151, 697–713.

Westaway, R., 2002. Seasonal seismicity of northern California before the great 1906 earthquake. Pure and Applied Geophysics 159, 7-62.

Westaway, R., 2006. Investigation of coupling between surface processes and induced flow in the lower continental crust as a cause of intraplate seismicity. Earth Surface Processes and Landforms 31, 1480-1509.

Westaway, R., 2009. Quaternary uplift of northern England. Global and Planetary Change, 68, 357-382.

Westaway R., 2010. Cenozoic uplift of southwest England. Journal of Quaternary Science, 25, 419-432.

Westaway R., 2015a. Induced seismicity. In: Environmental and Health Issues in Unconventional Oil and Gas Development, Edited by: Debra Kaden and Tracie L. Rose. Elsevier, Amsterdam, pp. 175-210.

Westaway R., 2015b. Review of 'Caves and Karst of the Yorkshire Dales, Volume 1, edited by Tony Waltham and David Lowe.' British Cave Research Association, Buxton, 2013, 264 pp. Quaternary Science Reviews, 126, 276-277.

Westaway R., 2016a. The importance of characterizing uncertainty in controversial geoscience applications: induced seismicity associated with hydraulic fracturing for shale gas in northwest England. Proceedings of the Geologists' Association, 127, 1–17.

Westaway, R., 2016b. Some additional thoughts on Preese Hall. Solid Earth Discussions, Interactive Discussion item SC10, 9 pp. Available online: http://www.solid-earth-discuss.net/se-2015-134/discussion (accessed 13 August 2016)

Westaway R., 2017. Isostatic compensation of Quaternary vertical crustal motions: coupling between uplift of Britain and subsidence beneath the North Sea. Journal of Quaternary Science, in press. doi: 10.1002/jqs.2832.

Westaway, R., Bridgland, D.R., White, M.J., 2006. The Quaternary uplift history of central southern England: evidence from the terraces of the Solent River system and nearby raised beaches, Quaternary Science Reviews, 25, 2212-2250.

Westaway, R., Bridgland, D.R., White, T.S., Howard, A.J., White, M.J., 2015. The use of uplift modelling in the reconstruction of drainage development and landscape evolution in the repeatedly glaciated Trent catchment, English Midlands, UK. Proceedings of the Geologists' Association, 126, 480–521.

Westaway, R., Younger, P.L., 2014. Quantification of potential macroseismic effects of the induced seismicity that might result from hydraulic fracturing for shale gas exploitation in the UK. Quarterly Journal of Engineering Geology and Hydrogeology, 47, 333–350.

Withjack, M.O., Olson, J., Peterson, E., 1990. Experimental models of extensional forced folds. AAPG Bulletin, 74, 1038-1054.

Woodcock, N.H., Fischer, M., 1986. Strike-slip duplexes. Journal of Structural Geology, 8, 725-735.

Younger, P.L., 2016a. How can we be sure fracking will not pollute aquifers? Lessons from a major longwall coal mining analogue (Selby, Yorkshire, UK). Earth and Environmental Science Transactions of the Royal Society of Edinburgh, 106, 89-113.

Younger, P.L., 2016b. Interactive comment on "Hydraulic fracturing in thick shale basins: problems in identifying faults in the Bowland and Weald Basins, UK" by David K. Smythe. Solid Earth Discussions, Interactive Discussion item SC6, 8 pp. Available online: http://www.solid-earth-discuss.net/se-2015-134/discussion (accessed 21 August 2016)

Zhang ZhaoBin, Li Xiao, 2016. The shear mechanisms of natural fractures during the hydraulic stimulation of shale gas reservoirs. Materials, 9, 713, 14 pp. doi: 10.3390/ma9090713